# Modulation of piezoelectric properties in electrospun PLLA nanofibers for application-specific self-powered stem cell culture platforms

Youyi Tai[1#], Steve Yang[2#], Sooyoun Yu[3], Aihik Banerjee[1], Nosang V. Myung[3*], Jin Nam[1,2*]

[1] Department of Bioengineering, University of California-Riverside, Riverside, CA92521, USA

[2] Program of Materials Science and Engineering, University of California-Riverside, Riverside, CA92521, USA

[3] Department of Chemical and Biomolecular Engineering, University of Notre Dame, Notre Dame, IN 46556, USA

[#]: Y.T. and S.Y. contributed equally to this work.

*: corresponding authors

Prof. Nosang V. Myung
Department of Chemical and Biomolecular Engineering
University of Notre Dame
Notre Dame, IN 46556
1-574-631-3468
nmyung@nd.edu

Prof. Jin Nam
Department of Bioengineering
University of California-Riverside
Riverside, CA92521
1-951-827-2064
jnam@engr.ucr.edu

**Abstract**

There is an increasing effort to utilize piezoelectric materials as a self-powered platform to electrically stimulate cells/tissues in regenerative medicine and tissue engineering applications. Poly(l-lactic acid) (PLLA) holds great potential for biological applications due to its biodegradability, especially in a nanofibrous form prepared by electrospinning. However, the mechanism underlying its realization and transformation of piezoelectricity is not well understood. In this study, a design-of-experiment approach was employed to systematically dissect the effects of dimensional control and heat treatment on the piezoelectric performance of electrospun PLLA nanofibers. Specifically, we revealed that the fiber diameter- and heat treatment-dependent phase content change between electrospinning-induced amorphous and crystalline α/α' phases was responsible for the piezoelectric performance in the transverse and longitudinal directions. Such modulation of piezoelectric properties in PLLA nanofibers was critical in determining the differentiation efficiency of stem cells in a phenotype-specific manner, where neurogenesis and osteogenesis were enhanced by orthogonal and shear piezoelectricity, respectively. Overall, our findings highlight the potential of electrospun PLLA nanofibers with precisely controlled piezoelectric properties through a systematic approach for self-powered stem cell engineering platforms, specific to target tissues.

**Keywords:** Poly(l-lactic acid), electrospinning, piezoelectricity, self-powered, stem cells

## 1. Introduction

There is a growing interest in utilizing piezoelectric materials in diverse applications including sensors, actuators, energy harvesting electronics, and bio-implants [1]. The direct piezoelectric effect allows the material to exhibit a charge separation in response to external mechanical stress, useful for its applications in sensing or energy harvesting [2], [3], [4]. On the other hand, under the reverse piezoelectric effect, an applied external electric field induces a mechanical strain, which provides potential applications in mechanical actuators [1]. Recently, such direct- or reverse-piezoelectric energy conversions found their utility in various biological applications including biosensors, bioactuators, and drug delivery platforms [5], [6], [7]. Particularly, due to the innate bioelectrical activity and piezoelectricity in various tissues of the body including nerve, bone, dentin, cartilage, and ligaments, there is an increasing effort to utilize piezoelectric materials as a self-powered platform to electrically stimulate cells/tissues in regenerative medicine and tissue engineering applications [8], [9], [10], [11], [12], [13]. In this context, inorganic piezoelectric materials such as lead zirconate titanate (PZT), aluminum nitride (AIN), zinc oxide (ZnO), and barium titanate ($BaTiO_3$) exhibit excellent piezoelectric coefficients enabling the activation of the piezoelectric effect under physiologically safe mechanical perturbation [14], [15], [16]. However, their brittle nature limits their applications in low frequency, high strain conditions, typical for *in vivo* biological environments. In contrast, organic piezoelectric materials, which are mechanically flexible, provide an alternative opportunity for addressing the limitations of inorganic piezoelectric materials.

Polyvinylidene fluoride (PVDF) and its derivatives have been heavily investigated for their excellent piezoelectric properties exhibiting the highest piezoelectric coefficient of $d_{33}$ up to -108 $pm \cdot V^{-1}$ when properly processed [17], comparable to those of inorganic materials. Its high

piezoelectric performance and good flexibility have enabled the use of PVDF-based materials in a variety of applications including bio-sensors, wearable nanogenerators, and tissue engineering and regenerative medicine [18], [19], [20]. In comparison, poly(l-lactic acid) (PLLA) possesses a different main polarization direction of the piezoelectric domain, exhibiting the highest value of the shear piezoelectric coefficient of $d_{14}$ at approximately 12 pm·V$^{-1}$ [6]. The thermodynamically stable conformations of PLLA in ambient conditions are the α and α'-crystalline forms, where the -CO-O dipoles are helically oriented along the main backbone chain [21], [22]. When this helix structure is sheared through its side chain, a slight re-orientation of the -CO-O dipoles occurs, inducing the polarization of the chain molecules [22]. The direction of the polarization is parallel to the plane of applied shear stress that results in the shear piezoelectricity of the polymer. Owing to its unique piezoelectric direction, PLLA has greater utility in the applications where the primary mode of mechanical actuation is under shear, as compared to PVDF and its derivatives which lack responsiveness to shear strains [6]. Furthermore, its biodegradability further motivates its utilization in niche areas, for example, bone tissue engineering where its shear piezoelectricity is particularly relevant to the native electrical environment derived from the uniaxially aligned, shear-responsive collagen structure in bone [23], [24].

We have previously shown that electrospinning enhances the piezoelectric properties of P(VDF-TrFE) nanofibers in a fiber size-dependent manner due to the alternation in electroactive phase contents and piezoelectric domain alignment under the influence of high electric fields and mechanical stretching during the electrospinning process [3]. Interestingly, several studies have shown that electrospinning enables PLLA to align its dipoles perpendicular to the fiber direction, forming an amorphous or electrospun phase [25]. The emergence of the electrospinning-induced amorphous phase realizes the piezoelectric effect normal to the fiber orientation, which is similar

to PVDF and most of the inorganic piezoelectric materials [25], [26]. A few studies have shown that heat treatment of electrospun PLLA fibers will affect its piezoelectric properties, likely due to the change of the amorphous phase to crystalline phases [24], [27], [28]. However, these studies were limited in phenomenological observations, lacking a fundamental understanding of piezoelectric mechanisms that may guide methodologies to engineer and further improve the piezoelectric properties of PLLA.

Herein, we used a systematic approach to optimize the electrospinning process for the synthesis of aligned PLLA nanofibers with different fiber diameters ranging from 30 to 500 nm. They were subjected to various heat treatment regimens to manipulate crystal structures and their resulting electrical outputs were investigated. The fiber diameter- and heat treatment-dependent phase changes, determined from differential scanning calorimetry (DSC) and Fourier-transform infrared spectroscopy (FTIR), were correlated to the piezoelectric performances, augmented by piezoresponse force microscopy (PFM). We further investigated how such a difference in piezoelectric performance, especially piezoelectric domain orientation, modulated via dimensional control and heat treatment, affects stem cell behaviors. These results provide guidance to design and engineer PLLA nanofiber by exploiting the precisely controlled piezoelectric effects for specific biological applications.

## 2. Materials and Methods

### 2.1. Synthesis of electrospun PLLA nanofibers

A systematic approach by controlling electrospinning solution properties such as viscosity, electrical conductivity, and surface tension, was used to synthesize PLLA nanofibers with specific average fiber diameters. PLLA (Polyscience Corp., Niles, IL) was dissolved in a 70/30 volume

ratio mixture of dichloromethane (DCM) (Sigma-Aldrich, St Louis, MO) to N,N-dimethylformamide (DMF) (Fisher Scientific, Pittsburgh, PA) at 7 wt.%, 6 wt.%, 4.2 wt.%, and 1.9 wt.% to synthesize nanofibers with the target average fiber diameter of 500, 250, 150, and 30 nm, respectively. An equimolar mixture of pyridine and formic acid (PF) at 3 wt.% (Sigma-Aldrich, St Louis, MO) was added into the solutions.

Each solution was separately loaded into a 10 ml syringe attached with a 25-gauge needle. The solution was then electrospun for 4 hours at an applied voltage of 17 kV with a distance of 10 cm between the needle and rotating drum collector at 23 °C and humidity of 8.4 g $m^{-3}$. The solution feed rate was controlled at 0.5 ml $h^{-1}$ by a syringe pump (New Era Pump Systems, Inc., Farmingdale, NY). The rotating drum was set at an angular speed of 38.32 m $s^{-1}$ to produce nanofiber mats with aligned fibrous structures. The resulting PLLA fibrous mats were subjected to heat treatment for 12 hours in a rapid thermal annealing oven (Allwin21 Corp, Morgan Hill, CA) at various temperatures and quenched in a cold ethanol solution.

2.2. Characterization of electrospinning solutions and resulting nanofibers

The viscosity, electrical conductivity, and surface tension of the electrospinning solutions were characterized using a viscometer (Brookfield Engineering Laboratories, Inc., Middleboro, MA), a 4-cell conductivity probe (Fisher Scientific, Pittsburgh, PA), and a surface tensiometer (SKZ1013, Shandong Industrial, China), respectively. The morphology of the synthesized electrospun nanofibers from those solutions was characterized using a VEGA3 scanning electron microscope (SEM) (Tescan Brno, Czech Republic). Fiber diameter and bead density were assessed using the ImageJ software.

2.3. Temperature-dependent phase transition analysis of electrospun PLLA nanofibers

The phase transition temperatures, including the glass transition temperature, the cold crystallization temperature, and the melting temperature of electrospun PLLA nanofibers having various fiber diameters were determined using a differential scanning calorimeter (NETZSCH DSC 214 Polyma, Wittelsbacherstraße 42, Germany). DSC curves were acquired by heating a sample from 25 °C to 220 °C at a heating rate of 10 °C $min^{-1}$ in the air.

The degree of crystallinity from each DSC curve was calculated using the following equation [29], [30], [31],

$$X_c = \frac{\Delta H_f^m - \Delta H_c^m}{\Delta H_f^{100\%}} \times 100$$

where $X_c$ is the degree of crystallinity (%), $\Delta H_f^m$ is the heat of fusion (J $g^{-1}$) determined by integration of melting peak, $\Delta H_c^m$ is the heat of cold crystallization (J $g^{-1}$) determined by integration of cold crystallization peak, $\Delta H_f^{100\%}$ is the heat of fusion for 100% crystallized PLLA material (93.1 J $g^{-1}$) [32].

2.4. Electrical output measurements

Electrospun aligned PLLA nanofibrous mats (an approximate thickness of 30 μm) having an average fiber diameter of 30, 150, 250, or 500 nm, were subjected to various heat treatment regimens, followed by electrical output measurements using a vibrational system modified from our previous report [3]. Briefly, a cantilever setup was adopted to induce a controlled strain on the electrospun samples. The cantilever was composed of two 7.2 × 1.6 × 0.01 $cm^3$ brass shims covered on both sides with polyimide tape to electrically isolate them. A 4 × 1.2 $cm^2$ sample was cut from the electrospun nanofiber mat. Voltage outputs in two different directions, either

transverse ($V_3$; through the thickness of the sample) or longitudinal ($V_1$; along the aligned direction of the fibers) to the plane of the substrate, were measured. To measure $V_3$, the sample was fixed to the center of the cantilever with double-sided copper tapes which served as the bottom and top electrodes (**Figure S1a**). To measure $V_1$, two regions with a size of 0.5 × 1.2 $cm^2$ at both ends of the sample were connected to both sides of the brass plates using silver paste while the remaining part of the sample was insulated with polyimide tape (**Figure S1b**). 24-gauge electric wires were attached to the electric contacts, sealed with a strip of polyimide tape. An oscilloscope (Picoscope 2204A ™, Pico Technology Ltd.) was used to measure voltage outputs from the nanofiber mats. The applied strain for electrical output measurements to both directions was fixed at 0.18% with a frequency of 10 Hz.

2.5. Piezoelectric characterization

PFM was used to measure the piezoelectric coefficient, $d_{33}$, of single PLLA nanofibers. Briefly, a gold-coated silicon substrate was used to collect electrospun PLLA nanofibers. An MFP-3D atomic force microscopy (AFM, Asylum Research, Santa Barbara, CA) was used in a contact mode to locate an individual PLLA nanofiber. Subsequently, it was changed to a PFM mode where 3 separate points were selected to perform a single-point spectroscopy measurement along the length of each fiber. A step voltage was applied through the top of the fiber via an AFM probe (AC240TM, Olympus) to the grounded silicon substrate, and the corresponding amplitude change was recorded. The value of $d_{33}$ was then calculated using the following equation,

$$d_{33} = \frac{A}{VQ} f$$

where $A$ is the amplitude detected from the PFM probe after applying the step voltage, $V$ is the value of the applied voltage, $Q$ is the quality factor determined by both the sample and the probe,

and $f$ is the correctional factor derived from the periodically poled lithium niobate (PPLN) standard sample [33].

Additionally, phase scanning images were acquired during the AFM contact mode scanning. Phase angle values at each point along the length of the fiber were further subjected to histogram analysis. At least three fibers were used for each histogram analysis.

### 2.6. Phase content assessment of electrospun PLLA nanofibers

Fourier-transform infrared (FTIR) spectroscopy in the absorbance mode from 600 to 1600 $cm^{-1}$ (Nicolet 6700 FTIR spectrometer, Thermo Scientific., MA) was utilized to analyze the phase contents in PLLA nanofiber mats with different fiber diameters, subjected to various heat treatment regimens. X-ray diffraction (XRD) patterns from each sample were collected from 2θ of 10–30° using an Empyrean X-ray diffractometer (PANalytical, Almelo, the Netherlands). The baseline subtraction and peak deconvolution of FTIR and XRD data were processed using the OriginPro 8.5 software.

### 2.7. Stem cell culture on PLLA nanofibers

Electrospun PLLA nanofibers having an average fiber diameter of 150 nm and a thickness of 30 μm were used for stem cell culture. Electrospun PLLA nanofiber mat was cut to a dimension of 10x10 $mm^2$ and attached to the bottom of the cell culture plate using a medical adhesive (Factor II, Inc, AZ). The nanofiber mats were incubated in 70% ethanol for 30 minutes and then dried under UV exposure before cell seeding.

All experiments involving human stem cells were approved by UC Riverside Institutional Review Board (IRB; HS11-124) and Stem Cell Research Oversight (SCRO; SC20210002)

Committee. Human neural stem cells (hNSCs) derived from Riv9, an induced pluripotent cell line [34], were cultured in hNSC growth media composed of 50% Neurobasal medium (Gibco), 50% advanced DMEM/F12 (Gibco) with Neural induction supplement (Gibco) [35], [36]. All hNSCs used in this study were at passage 7. Briefly, hNSCs with a cell density of 20,000 cells $cm^{-2}$ were seeded on electrospun PLLA nanofibers having a fiber diameter of 150 nm with or without heat treatment at 65°C (heat-treated and as-spun, respectively). The hNSC growth media was used during the entire culture duration. The cells were subjected to either 4% paraformaldehyde (PFA) fixation for immunofluorescence imaging or lysed for gene expression analysis after 1 week of culture.

Human fetal bone marrow derived mesenchymal stem cells (hMSCs, Applied Biological Materials, Richmond, Canada) were cultured in hMSC growth media composed of DMEM-F12 (Gibco) supplemented with 15 % fetal bovine serum (VWR), 1% penicillin-streptomycin (Fisher), and 100 ng $mL^{-1}$ bFGF (PeproTech). Passage 6 of hMSCs was used in this study. Briefly, hMSCs with a cell density of 10,000 cells $cm^{-2}$ were inoculated on as-spun or heat-treated PLLA nanofibers. The cells were cultured in hMSC growth media for a day after seeding, followed by media exchange to osteogenic differentiation media, composed of low-glucose DMEM (Corning) supplemented with 10 % FBS, 10 mM sodium-β-glycerophosphate (Sigma), 200 μM ascorbic acid-2-phosphate (Sigma), 100 nM dexamethasone (Sigma), and 1% penicillin-streptomycin-fungizone (Sigma). The cells were either lysed for gene expression analysis after 1 week of culture or fixed in 4% PFA for histological staining after 2 weeks.

### 2.8. Characterization of stem cell differentiation

Fixed hNSC samples were immuno-stained with a primary antibody marker specific for neurons (Tuj. 1, Fisher) with an appropriate secondary antibody (m-IgGκ BP-CFL 488, Santa Cruz Biotechnology), followed by counter-staining with DAPI (Sigma) and phalloidin (Alexa Fluor-594, Abcam) for the visualization of nucleus and cytoskeleton, respectively. The stained samples were examined under a fluorescence microscope (DP80, Olympus). For hMSC samples, alizarin red S staining (Sigma) was used to determine osteogenic calcium deposition. Briefly, each fixed sample was incubated in 0.05% alizarin red solution before rinsing with DI water, mounting, and observing under a microscope (DP80, Olympus).

The neuronal differentiation of hNSCs and the osteogenic differentiation of hMSCs were further examined at the gene level by quantitative polymerase chain reaction (qPCR). RNA was extracted using an RNeasy Micro Kit (Qiagen, Valencia, CA) followed by cDNA synthesis using an iScript cDNA Synthesis Kit (Bio-rad, Hercules, CA). Real time-qPCR was performed to determine the gene expression of phenotypic markers (**Table S1**). The data were analyzed by the comparative threshold cycle ($C_T$) method using the expression of *GAPDH* as an endogenous control.

2.9. Statistical analysis

All experiments were conducted at a minimum of triplicate (n = 3), and data are represented as mean ± standard deviation. Each set of data was subjected to statistical analysis using SPSS (v.19.0) to either determine significance by one-way analysis of variance (ANOVA) with Tukey's HSD posthoc or evaluate data correlation by Pearson's correlation coefficient ($r_p$). A value of $p \leq 0.05$ was regarded as statistically significant. For the strength of data correlation, it is generally

considered to be a strong correlation when $r_p \geq 0.7$, a moderate correlation when $r_p$ is between 0.4 and 0.69, and a weak correlation when $r_p \leq 0.39$ [37].

## 3. Results and Discussion

In this study, we aimed to examine how the piezoelectric properties of electrospun PLLA nanofibers impact their biological applications, i.e., as a self-powered cell culture platform. We particularly focused on the mechanisms underlying the modulation of piezoelectric orientation and magnitude in PLLA nanofibers via dimensional control and heat treatment. We further investigated how such modulation of piezoelectric properties affects the differentiation behaviors of stem cells in a cell type-specific manner.

We have previously demonstrated that the morphology of electrospun piezoelectric nanofibers, i.e., fiber diameter, is a significant factor in determining the piezoelectric efficiency in various materials [3], [38]. In order to determine the dimensional effect in electrospun PLLA nanofibers, a design of experiment (DOE) was employed to precisely control the fiber diameter and to eliminate defects (*i.e.*, beads). A two-level full factorial analysis with three factors, including PLLA, PF, and BYK-377 concentrations, was designed to determine their effects on fiber morphologies such as fiber diameter and fiber fraction (**Table S2**). The initial high and low concentrations of PLLA in this DOE were based on our previous work [3]. Briefly, PLLA concentration, used to primarily control viscosity, was set high at 6 wt.% when a solution exhibited a stable Taylor cone with little bead formation during electrospinning while the low PLLA concentration was determined when an unstable Taylor cone resulted in substantial bead formation (4 wt.%). The high concentration of PF, a salt, was set at 3 wt.% to significantly increase the solution electrical conductivity while maintaining the solubility of PLLA. The high concentration

of BYK-377, a surfactant, at 0.1 wt.% was determined where the surface tension was significantly reduced. Both of the low limits for PF and BYK-377 concentrations were set at 0. The center point of the DOE was prepared with an electrospinning solution of 5 wt.% PLLA, 1.5 wt.% PF, and 0.05 wt.% BYK-377, each of which was a mid-point between the high and low concentrations. These 9 conditions exhibited the expected trends in solution properties, including PLLA concentration-dependent solution viscosity, PF concentration-dependent solution conductivity, and BYK-377 concentration-dependent solution surface tension (**Table S2**). Electrospinning of these solutions resulted in various fiber morphologies (**Figure 1a-i**). The fiber diameter was most significantly influenced by the PLLA concentration, which independently controlled the solution viscosity and increased as PLLA concentration increased, ranging from approximately 130 to 300 nm (**Figure 1j, k**). In contrast, the fiber fraction was most significantly influenced by the PF concentration, which controlled the solution conductivity (**Figure 1l, m**). Smaller bead density or higher fiber fraction was achieved approximately at 99% when 1 wt.% PF was used (**Figure 1a, c, e, g**) while the fiber fraction was relatively low at 79% in the absence of PF (**Figure 1b, d, f, h**). The BYK-377 concentration, however, showed little effect on fiber morphology probably because the electrospinning solution exhibited low enough surface tension in the absence of BYK-377 to form a stable Talyor cone during electrospinning. Additionally, the factor analysis showed minimal effects from the combination of the three factors on either fiber diameter or fiber fraction (**Figure 1k, m**). The linearity of the factor analysis was confirmed by electrospinning the DOE center point solution, producing PLLA nanofibers with an average fiber diameter of 244 ± 39 nm, close to the expected value of 221.5 nm (**Figure 1i**).

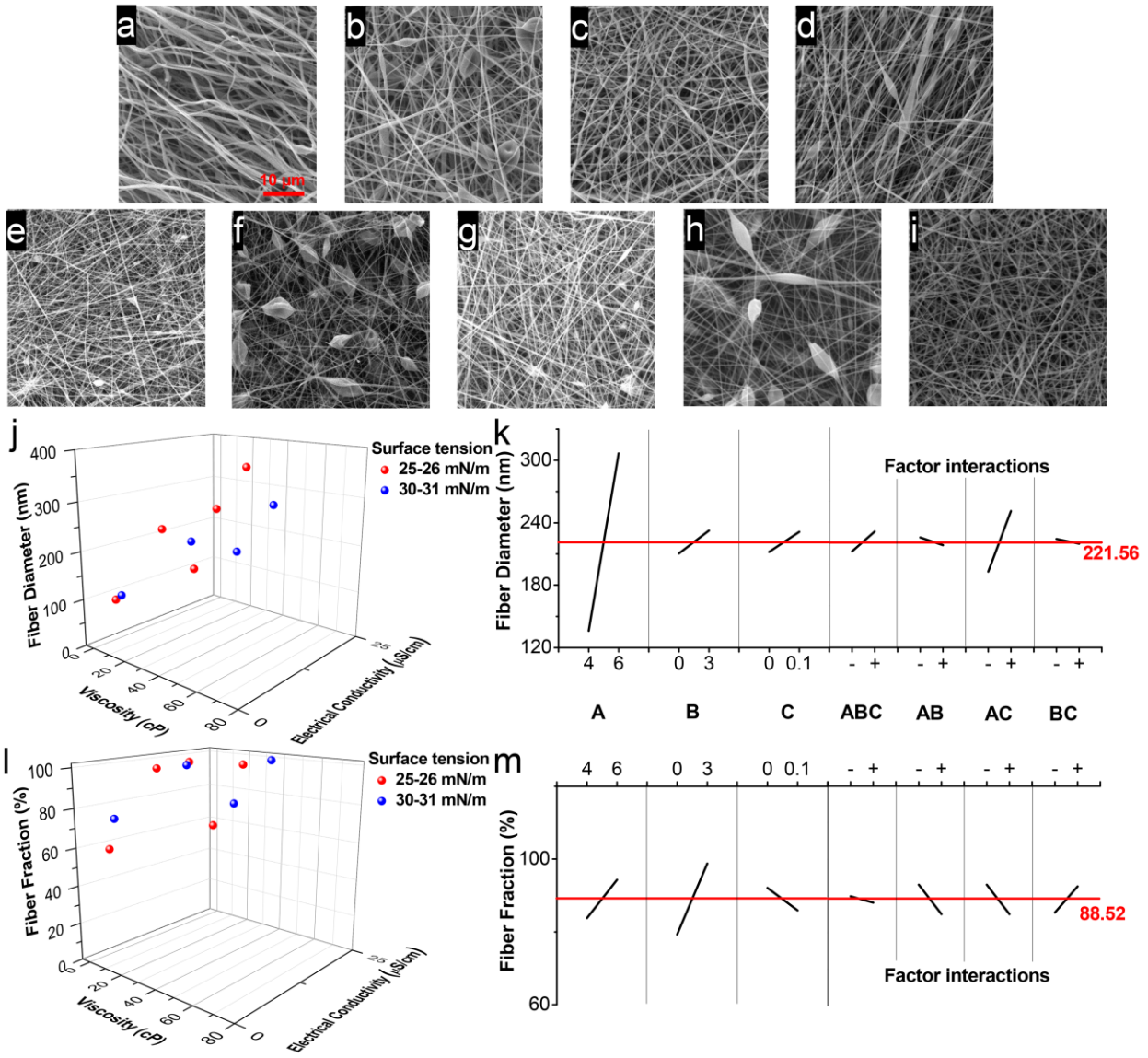


**Figure 1. Effects of electrospinning solution properties on the morphology of PLLA nanofibers.** (a-i) SEM images showing representative PLLA nanofiber morphologies resulted from a design-of-experiment (DOE) with variables of PLLA, PF, and BYK-377 concentrations that primarily modulate viscosity, electrical conductivity, and surface tension, respectively, of the electrospinning solution properties (see Table S2). 6 wt.% PLLA (a-d), 4 wt.% PLLA (e-h), 3 wt.% PF (a, c, e, g), 0 wt.% PF (b, d, f, h), 0.1 wt.% BYK-377 (a, b, e, f), 0 wt.% BYK-377 (c, d, g, h), and the midpoint of 5 wt.% PLLA solution with 1.5 wt.% PF and 0.05 wt.% BYK-377 (i). (j, l) Effects of electrospinning solution properties including viscosity, electrical conductivity, and surface tension on fiber diameter and fiber fraction. (k, m) DOE factor analysis on fiber diameter and fiber fraction. Red lines indicate average values. A, B, and C denote PLLA, PF, and BYK-377 concentrations (wt.%), respectively.

Based on the DOE analysis, aligned PLLA nanofibers having an average fiber diameter of approximately 30 nm, 150 nm, 250 nm, or 500 nm were electrospun by using electrospinning solutions with the PLLA concentration at 7 wt.%, 6 wt.%, 4.2 wt.%, and 1.9 wt.%, respectively (**Figure 2a-h**). Additionally, 3 wt.% of PF was added to all electrospinning solutions to keep a uniform fiber morphology. Since there was no significant effect of surface tension on either fiber diameter or fiber fraction, BYK-377 was not added into the electrospinning solutions. PLLA nanofibers with a larger average diameter exhibited a greater degree of alignment with a significant deviation of uniaxial alignment in 30 nm nanofibers from other samples (**Figure 2i-l**). This may be attributed to the airflow generated from the collector rotating at a high speed to align nanofibers, differentially affecting nanofiber collection; smaller fibers with lower masses are easily influenced by the airflow, resulting in a more randomly oriented fiber collection.

In order to determine heat treatment regimens, electrospun PLLA nanofibers having various fiber diameters were subjected to DSC analysis (**Figure 2m**). Regardless of fiber diameter, all DSC curves showed a similar pattern where an endothermic peak was observed at 66.8 °C for 30nm and 150 nm, 66.7 °C for 250 nm, and 65.4 °C for 500 nm, corresponding to the glass transition temperature of electrospun PLLA nanofibers. An exothermic peak at approximately 77 °C was observed immediately after the glass transition peak, indicating the "cold crystallization" of the materials during the process. Melting took place between 150 and 182 °C and it peaked approximately at 177 °C [39], [40], [41]. From these results, a range of heat treatment regimens from 22 °C to 135 °C, which underwent the glass transition and "cold crystallization" before the start of melting, was determined. Interestingly, the DSC data showed the fiber size-dependent crystallinity of PLLA nanofibers; the crystallinity proportionally increased as the fiber diameter increased where the nanofibers with an average fiber diameter of 30 nm exhibited approximately

40% crystallinity while that of 500 nm-nanofibers exhibited approximately 48%. This trend was opposite to our previous results in P(VDF-TrFE) where the dimensional reduction enhanced the crystallinity of the nanofibers [3].

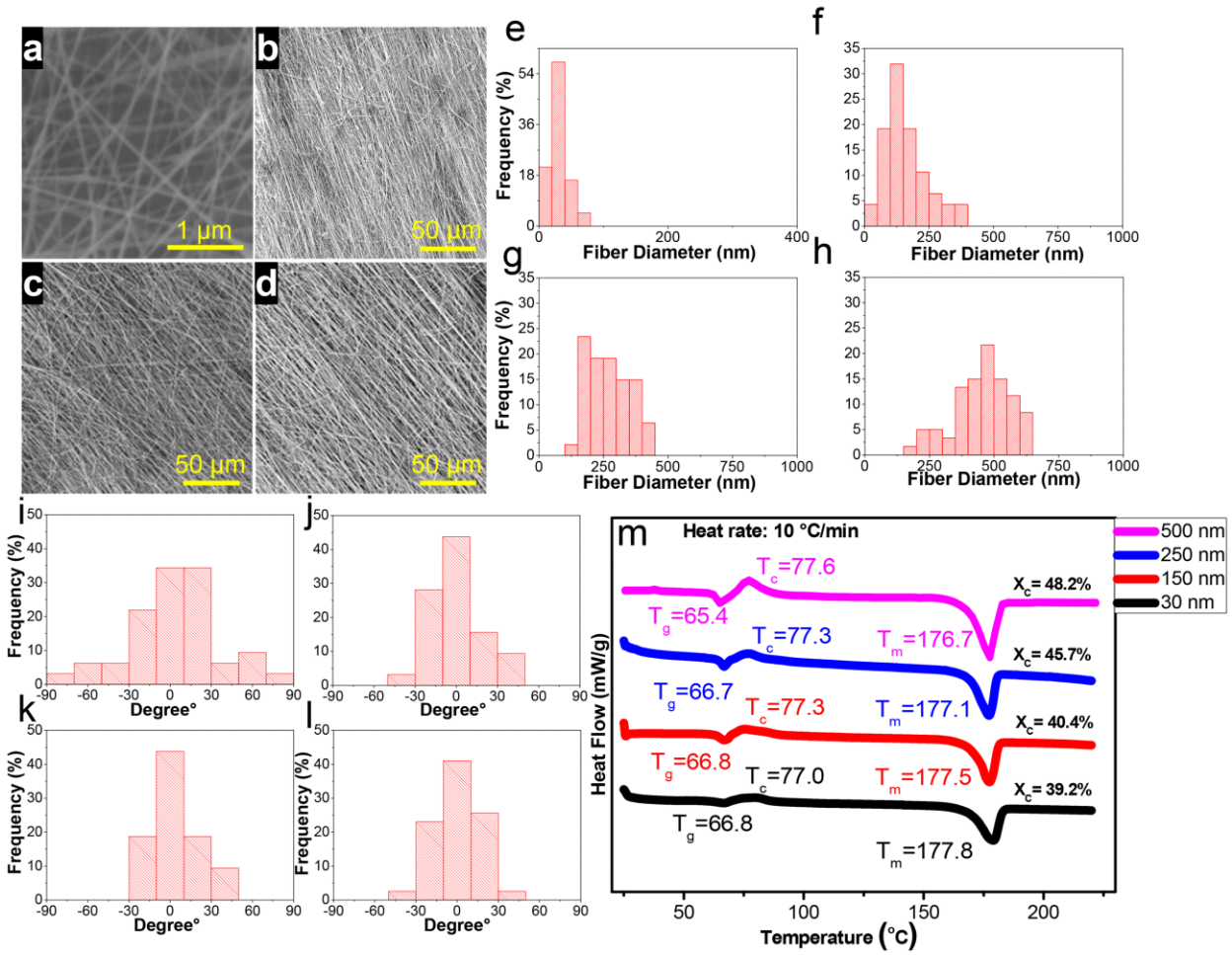


**Figure 2. Morphological and thermal characterization of electrospun PLLA nanofibers with various fiber diameters.** (a-d) Representative SEM images and (e-h) fiber diameter histograms of electrospun aligned PLLA nanofibers having an average diameter of approximately (a, e) 30 nm, (b, f) 150 nm, (c, g) 250 nm, or (d, h) 500 nm. (i-l) Corresponding fiber alignment histograms of electrospun PLLA nanofibers having an average fiber diameter of (i) 30 nm, (j) 150 nm, (k) 250 nm, or (l) 500 nm. (m) Representative DSC curves of electrospun PLLA nanofibers having different average fiber diameters.

We next investigated the fiber diameter- and heat treatment-dependent piezoelectric performance of electrospun aligned PLLA nanofibers under a controlled strain of 0.18% and a frequency of 10 Hz using a cantilever system as described earlier (**Figure S1**). The mat thickness

of the electrospun aligned PLLA nanofibers was 30 μm as shown in cross-sectional SEM images (**Figure S2**). The fiber diameter of PLLA nanofibers significantly affected the piezoelectric performance as the sample with an average fiber diameter of 30 nm produced almost 8-fold greater voltage outputs in the transverse direction ($V_3$) than that of 500 nm nanofibers (**Figure 3a**). Interestingly, there was a significant decrease in the transverse voltage outputs at a heat treatment temperature of 65 °C, which was near the glass transition temperature (66 °C) of electrospun aligned PLLA nanofibers determined by the DSC analysis. The decrease in $V_3$ coincided with a significant increase in longitudinal voltage output ($V_1$) of electrospun aligned PLLA nanofibers for all fiber diameters after heat-treatment at 65 °C (**Figure 3b**). Interestingly, a significant decrease in $V_1$ was observed after heat treatments at higher temperatures with its threshold temperature depending on the fiber diameter, where 30 nm and 150 nm nanofibers exhibited $V_1$ drop at 85 °C and 105 °C, respectively while $V_1$ of 250 and 500 nm nanofibers significantly decreased at 125 °C.

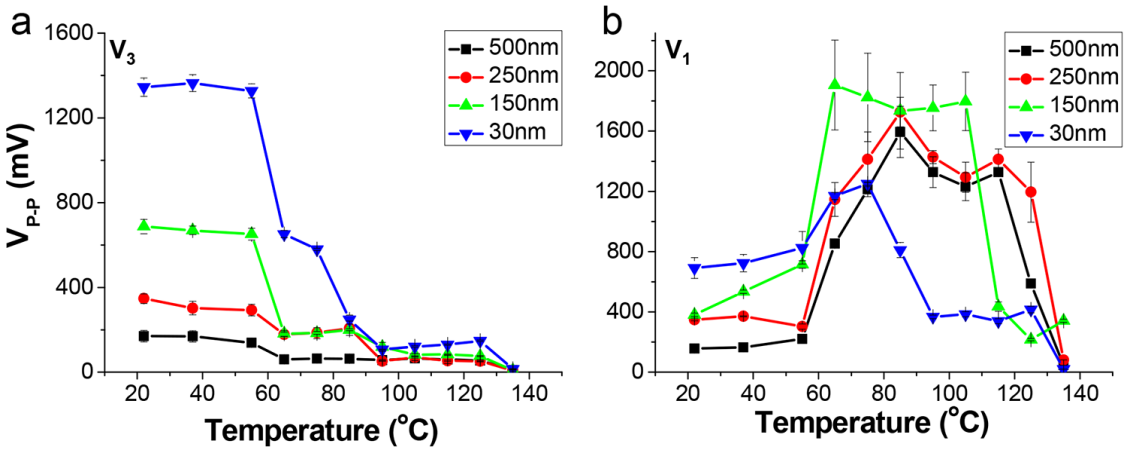


**Figure 3. Electrical outputs of electrospun PLLA nanofibers with various fiber diameters and heat treatments.** Peak-to-peak voltage outputs of electrospun aligned PLLA nanofiber mats (~30 μm thick) having an average fiber diameter of approximately 30, 150, 250, or 500 nm, subjected to various heat-treatment regimens in the (a) transverse direction ($V_3$) or (b) longitudinal direction ($V_1$).

In order to understand the mechanism underlying the fiber size-dependent $V_3$ of electrospun aligned PLLA nanofibers, the piezoelectric coefficient $d_{33}$ and piezoelectric dipole alignment of individual PLLA nanofibers were examined by PFM. Piezoelectric coefficient $d_{33}$, which is directly related to the $V_3$ value, was measured by single point PFM on as-spun PLLA nanofibers with fiber diameters ranging from 15 to 525 nm. Similar to our observation in other polymer systems [3], [17], an exponential increase of $d_{33}$ value was observed as the fiber diameter decreased, especially below 100 nm (**Figure 4a**). It should be noted that the average $d_{33}$ value of spin-coated PLLA film is significantly lower than those of electrospun PLLA nanofibers. The enhanced alignment of polymer chains by restricting the degree of freedom in chain movement due to electric poling and mechanical stretching during the electrospinning process likely induced this increased $d_{33}$ in electrospun PLLA nanofibers [42], [43]. Therefore, to further determine the effects of fiber morphology on polymer chain/piezoelectric dipole alignment, piezoelectric phase imaging was conducted on as-spun PLLA nanofibers with a fiber diameter of approximately 30, 150, 250, or 500 nm. Each fiber was first precisely located by AFM scanning (**Figure 4b**), after which the phase angle values were acquired along the length of the fiber (**Figure 4c**). The arch geometry on the top of the PLLA fibers caused the PFM tip to create an imaging artifact along the width of the fiber, in which the fiber appears wider than the actual fiber diameter in the scanned images. Therefore, height retrace graphs were used to determine the true location of the fiber. Three independent fibers per condition were used for phase distribution histograms (**Figure 4d-g**). The data showed that the standard deviations of phase angle distribution decreased from 28.73° to 1.42° when the fiber diameter decreased from 500 nm to 30 nm, indicating that the decrease in fiber size enhanced the alignment of the piezoelectric dipole orientation. The lower solution viscosity to produce a smaller fiber diameter likely induced less polymer chain entanglement and

greater polymer chain alignment [44]. Together with the increased formation of electrospinning-induced amorphous phase that is responsible for the materialization of orthogonal piezoelectric coefficient, therefore, smaller fiber dimensions result in greater piezoelectric dipole alignment, thus greater transverse voltage outputs.

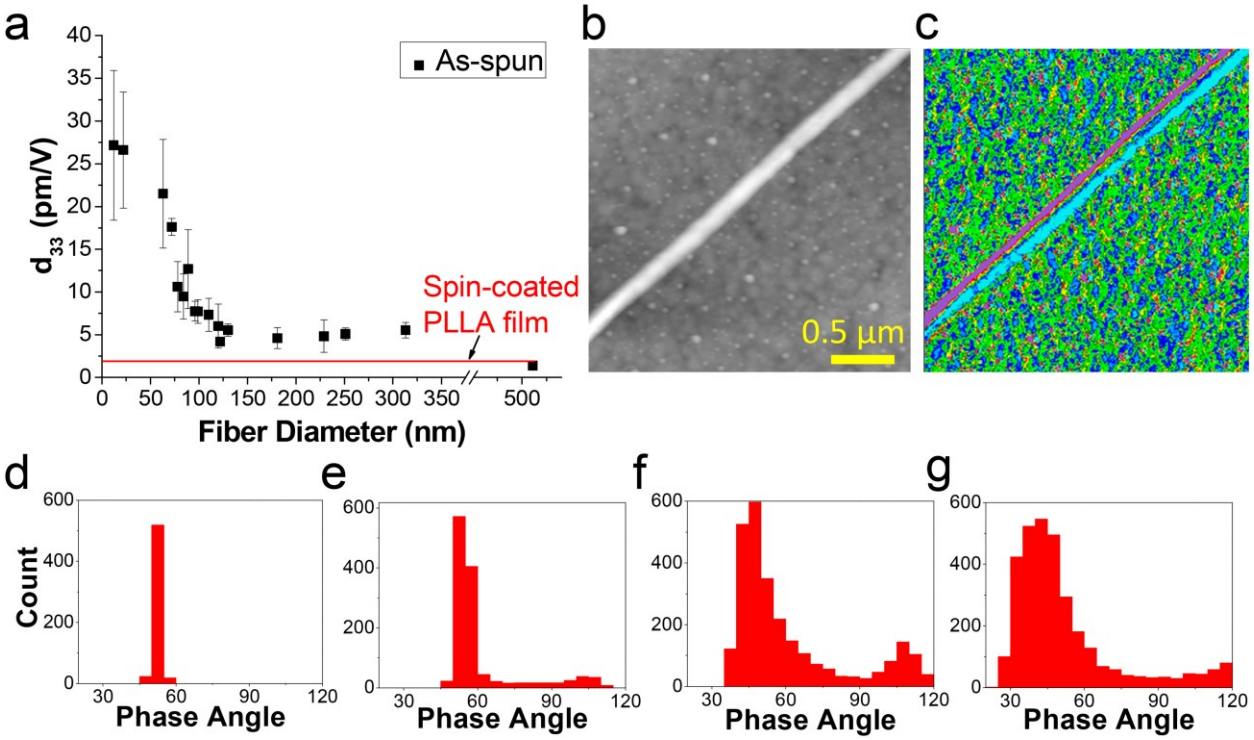


**Figure 4. Piezoelectric characterization of electrospun PLLA nanofibers with various fiber diameters.** (a) Piezoelectric coefficients ($d_{33}$) of as-spun PLLA nanofibers as a function of fiber diameter, measured by piezoresponse force microscopy (PFM). The red solid line indicates the $d_{33}$ value of spin-coated PLLA dense film. (b) A representative atomic force microscopy (AFM) image and (c) a corresponding piezoelectric phase angle image of an as-spun PLLA nanofiber having a fiber diameter of approximately 30 nm. (d-g) Phase angle histograms of as-spun PLLA nanofibers with a fiber diameter of approximately (d) 30 nm, (e) 150 nm, (f) 250 nm, and (g) 500 nm.

The fiber-size dependent piezoelectric performance in the transverse direction, $V_3$, however, diminished after heat treatment above the glass transition temperature. To determine the mechanism underlying the heat-treatment dependent piezoelectric performance, FTIR was used to quantify different electroactive phases of electrospun PLLA nanofibers with various fiber diameters, subjected to various heat treatment regimens. The electrospinning-induced amorphous

phase, responsible for $d_{33}$, and α and α' phases that contribute to the piezoelectric effect in the helical direction ($d_{14}$) were the focus of analysis [25], [26], [45]. Raw FTIR spectra of electrospun PLLA nanofibers having an average fiber diameter of 30 nm, 150 nm, 250 nm, or 500 nm, subjected to various heat-treatment regimens, are shown in **Figure S3**. Each individual FTIR spectrum was base-line subtracted (**Figure 5a**) and zoomed in near 1320-1400 $cm^{-1}$ band (**Figure 5b**) and 1150-1250 $cm^{-1}$ band (**Figure 5c**). These bands were deconvoluted to reveal the peak at 1365 $cm^{-1}$ (owing to -CH bending and $-CH_3$ bending) or 1213 $cm^{-1}$ (owing to $-CH_3$, -C=O vibration), which represents electrospun amorphous phase or α+α' phase, respectively. The intensity changes of the FTIR peaks at 1365 $cm^{-1}$ and 1213 $cm^{-1}$ with respect to fiber diameter and heat treatment were analyzed (**Figure 5d-k**). Generally, the intensity of the electrospun phase peak at 1365 $cm^{-1}$ decreased as heat treatment temperature increased (**Figure 5d-g**). Coinciding with the heat treatment-dependent $V_3$ drop in **Figure 3a**, the peak intensity decrease became more distinct above the glass transition temperature, indicating the decrease of amorphous phase content in electrospun PLLA nanofibers. This decrease in the peak intensity at 1365 $cm^{-1}$ corresponded to the peak intensity increase at 1213 $cm^{-1}$, signifying the increase of crystalline α and α' phases after being heat-treated above the glass transition and recrystallization temperatures (**Figure 5h-k**). The increase of peak intensity at 1213 $cm^{-1}$ was well correlated to the $V_1$ output increase in **Figure3b**. These peak intensity changes at 1365 $cm^{-1}$ and 1213 $cm^{-1}$ were further quantified to correlate with $V_3$ and $V_1$ outputs, respectively; the Pearson's coefficient values ($r_p$) of 0.941 (30 nm), 0.972 (150 nm), 0.930 (250 nm), and 0.824 (500 nm) indicated a strong dependence of $V_3$ output on amorphous phase content where the temperature-dependent decrease in $V_3$ corresponded to the decrease of electrospinning-induced amorphous phase content (**Figure 5l-o**). In addition, the increase in $V_1$ was consistent with the increase of α+α' phase content (**Figure S4**). These results

indicated that the relatively high $V_3$ outputs below the glass transition temperature of 65 °C were likely due to the greater amorphous phase content generated during the electrospinning process while the decrease of the phase content when heat treated above the glass transition temperature led to a reduction in $V_3$ outputs. Similarly, the relatively low $V_1$ outputs below 65 °C were due to a lack of α and α' phase content while the rearrangement of polymer chains into α and α' phase above the glass transition temperature resulted in the enhanced shear piezoelectricity, thus increased $V_1$ voltage outputs.

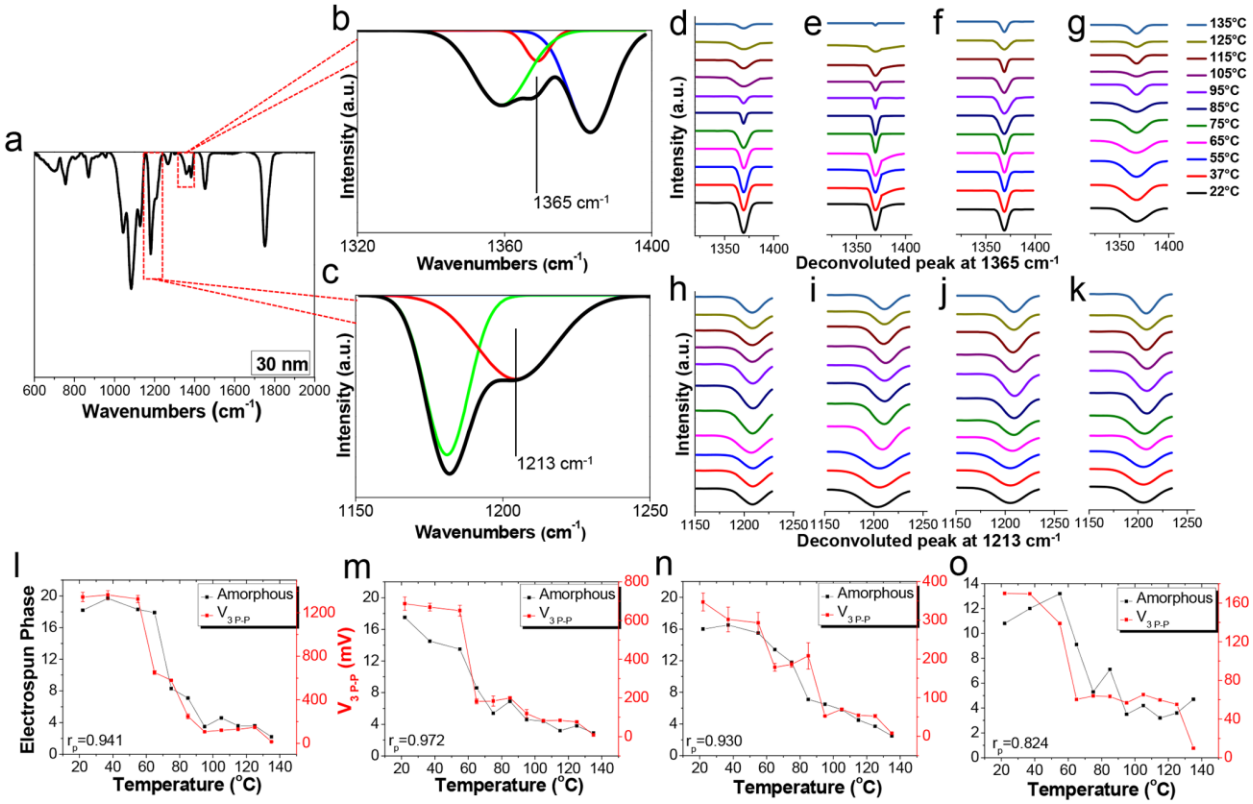


**Figure 5. FTIR analysis of electrospun PLLA nanofibers with various fiber diameters and heat treatments.** (a) A presentative FTIR spectrum of as-spun PLLA nanofibers having an average fiber diameter of 30 nm and its peak deconvolution near (b) 1320-1400 $cm^{-1}$ band and (c) 1150-1250 $cm^{-1}$ band. (d-k) Deconvoluted FTIR peaks of electrospun PLLA nanofibers having an average fiber diameter of (d, h) 30 nm, (e, i) 150 nm, (f, j) 250 nm, and (g, k) 500 nm, subjected to various heat-treatment regimens for (d-g) electrospun phase at 1365 $cm^{-1}$ and (h-k) α+α' phase at 1213 $cm^{-1}$. (l-o) Correlation between electrospun phase content and transverse voltage output ($V_3$) of electrospun aligned PLLA nanofibers with an average fiber diameter of (l) 30 nm, (m) 150 nm, (n) 250 nm, and (o) 500 nm, subjected to various heat treatment regimens ($r_p$ denotes the Pearson correlation coefficient).

While the decrease of $V_3$ and increase of $V_1$ were well correlated to the FTIR analysis, the significant voltage output drop of $V_1$ at 85 °C for 30 nm, 115 °C for 150 nm, and 125 °C for 250 and 500 nm nanofibers was not fully explained by the α+α' crystalline phase changes (**Figure S4**). Such weak correlation was also indicated by relatively low $r_p$ values (0.081, 0.535, 0.794, and 0.773 for 30, 150, 250, and 500 nm PLLA nanofibers, respectively) between α+α' phase content and $V_1$ output. In order to dissect the fiber diameter- and heat treatment-dependent changes in the crystal structure in detail, x-ray diffraction (XRD) was utilized (**Figure S5**). The significant increase in peak intensity near 2θ of 16.5° after heat treatment above 65 °C indicates the increase in the crystalline phase, corresponding to the α+α' phase content increase from the FTIR analysis. The XRD spectra (**Figure 6a**) were subjected to peak deconvolution to separate α' and α phases at 2θ of 16.4° and 16.7°, respectively (**Figure 6b**). A collection of fiber diameter- and heat treatment temperature-dependent peak intensity changes for α' and α phases is shown in **Figure 6c-j**. Both the α' and α phase contents, determined by the area under the peaks at 16.4° and 16.7°, respectively, increased as heat treatment temperature increased to 65 °C. At heat treatment temperature above 105 °C, however, a significant decrease in α' phase content was observed without a notable change in the α phase content. The change in α' phase content was well correlated to the $V_1$ output, especially for the sudden decrease of $V_1$ after the initial increase above the glass transition temperature, which could not be explained by the FTIR analysis (**Figure 6k-n** vs. **Figure S4a-d**). This better correlation between $V_1$ and α' phase content was also indicated by the higher $r_p$ values as compared to those between $V_1$ and α+α' phase content (**Figure S4a-d**). It should be noted that the area under the peak at 16.4° for 30 nm nanofibers decreased at a significantly lower heat treatment temperature as compared to that of 150, 250, and 500 nm fiber diameters, corresponding to the low $V_1$ value above 85 °C. This correlation between the α' phase content and

$V_1$ output suggests that α' phase is primarily responsible for the shear piezoelectric property of PLLA.

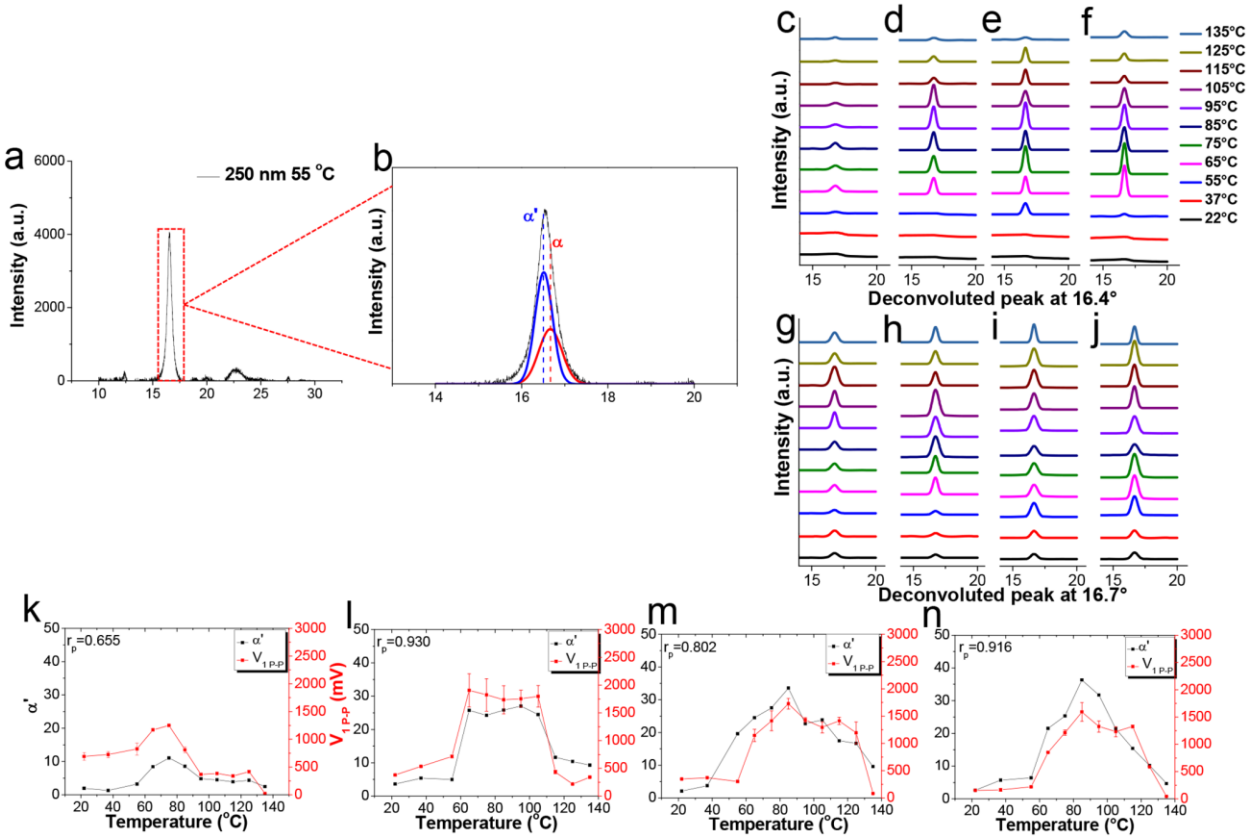


**Figure 6. XRD analysis of electrospun PLLA nanofibers with various fiber diameters and heat treatments.** (a) A presentative XRD pattern of 55 °C heat-treated electrospun PLLA nanofibers having an average fiber diameter of 250 nm and (b) its peak deconvolution for the α' (2θ: 16.4°) and α phase (16.7°) phases. (c-j) Deconvoluted XRD peaks of electrospun PLLA nanofibers having an average fiber diameter of (c, g) 30 nm, (d, h) 150 nm, (e, i) 250 nm, and (f, j) 500 nm, subjected to various heat treatment regimens for (c-f) α' phase at 16.4° and (g-j) α phase at 16.7°. (k-n) Correlation between α' phase content and longitudinal voltage output ($V_1$) of electrospun aligned PLLA nanofibers with an average fiber diameter of (k) 30 nm, (l) 150 nm, (m) 250 nm, and (n) 500 nm, subjected to various heat treatment regimens ($r_p$ denotes the Pearson correlation coefficient).

Based on our findings in the fiber diameter- and heat treatment-dependent phase change, thus piezoelectric property change of electrospun PLLA nanofibers, we next determined how such changes in piezoelectric orientation and magnitude affect a biological process, i.e., phenotype-specific differentiation of stem cells. Piezoelectric scaffolds/substrates have been utilized in various tissue engineering applications [46], [47]. It has been shown that the piezoelectric effect

self-powered by the deformation of scaffolds from cell contractile forces enhances the differentiation of stem cells towards neuronal or osteogenic phenotypes [48], [49]. Since those cell phenotypes are consistently stimulated by electrical signals in their native environments, it is reasonable to postulate that electrical stimulation from piezoelectric scaffolds would enhance the functional gain of such cells. However, the innate electrical environments of neurons and osteoblasts are quite different, where the surface potential alteration occurs in the cell membrane of neurons under action potential propagation while the collagen, which is aligned with the longitudinal direction of the bone, has shear piezoelectricity affecting osteoblasts [23], [50]. Therefore, we hypothesized that the piezoelectric orientation of PLLA nanofibers would affect the differentiation efficiency of stem cells in a phenotype-specific manner. To test our hypothesis, we utilized as-spun and 65°C heat-treated aligned PLLA nanofibers on neuronal differentiation of human neural stem cells (hNSCs) and osteogenic differentiation of human mesenchymal stem cells (hMSCs). PLLA nanofibers having an average fiber diameter of 150 nm were selected for the biological study because these nanofibers exhibited the best shear piezoelectric property after heat treatment at 65 °C as shown in **Figure 3b** while providing a reasonable fiber alignment (**Figure 2j**). The as-spun and heat-treated nanofibers were first subjected to piezoelectric phase scanning (**Figure 7a-d**). As compared to the as-spun fiber, no detectable piezoelectric domain orientation was observed in the heat-treated PLLA nanofibers likely due to the polymer chain rearrangement above the glass transition temperature, removing the electrospinning-induced piezoelectric dipole alignment (**Figure 7e, f**). Such heat treatment did not affect the mechanical properties of PLLA nanofibers, another factor that may affect the differentiation behavior of stem cells (**Figure S6**).

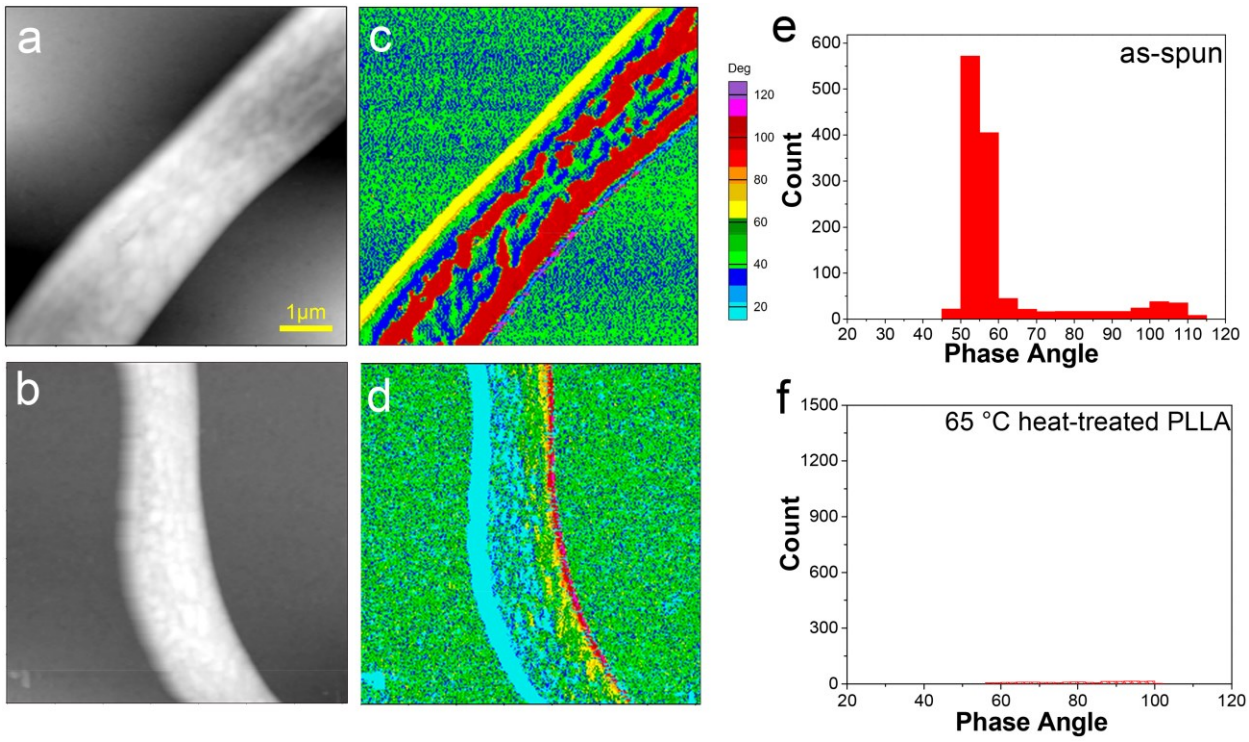


**Figure 7. Phase angle distribution of as-spun and 65 °C heat-treated PLLA nanofibers.** (a, b) AFM images and (c, d) piezoelectric phase angle images of (a, c) as-spun or (b, d) 65 °C heat-treated PLLA nanofiber with a fiber diameter of approximately 150 nm. (e, f) Phase angle histograms of (e) as-spun and (f) 65 °C heat-treated PLLA nanofibers with an average fiber diameter of 150 nm.

When hNSCs were cultured on these nanofibers with different piezoelectric orientations, a significant difference in differentiation efficiency was observed. The cells cultured on the as-spun nanofibers expressed a significantly greater amount of β3-tubulin, a neuronal marker, as compared to the cells cultured on either 6-well tissue culture plate or heat-treated nanofibers (**Figure 8a-d**). The gene expression of *TUBB3*, which encodes the protein of β3-tubulin, corroborated with the protein expression (**Figure 8e**). The expression of other genes, including early neuronal differentiation marker *NGN2*, intermediate neuronal marker *MAP2*, and mature neuronal marker *ENO2* exhibited the same pattern that these markers were significantly upregulated under the as-spun condition as compared to the heat-treated condition (**Figure 8f-h**). In contrast, osteogenic

differentiation of hMSCs was enhanced on the heat-treated nanofibers. A significantly greater amount of calcium deposition, indicating enhanced osteogenesis, was observed when the cells were cultured on the heat-treated nanofibers as compared to the control and as-spun conditions (**Figure 8i-l**). Consistent with the result of calcium deposition, osteogenic differentiation markers, including *RUNX2*, *ALPL*, *SPP1*, *BGLAP* were also upregulated on the heat-treated nanofibers (**Figure 8m-p**). When hNSCs were cultured on as-spun nanofibers, the mechanical contraction forces generated by the cell-matrix interaction through focal adhesion complexes would activate the piezoelectric PLLA nanofibers, with a $d_{33}$ value of approximately 5 $pmV^{-1}$ that produces a local piezoelectric potential in the range of 0.5-10 mV, sufficient for cell activation [51], [52], [53]. For highly mobile hMSCs, the heat-treated electrospun PLLA nanofibers that possess a high shear piezoelectric property would induce the piezoelectric effect originated from the shear force by cell elongation and migration, similar to the *in vivo* conditions of bone tissues [54]. Therefore, these results demonstrate that the piezoelectric orientation of the self-powered cell culture platform is critical in modulating cellular behaviors in a phenotype-specific manner.

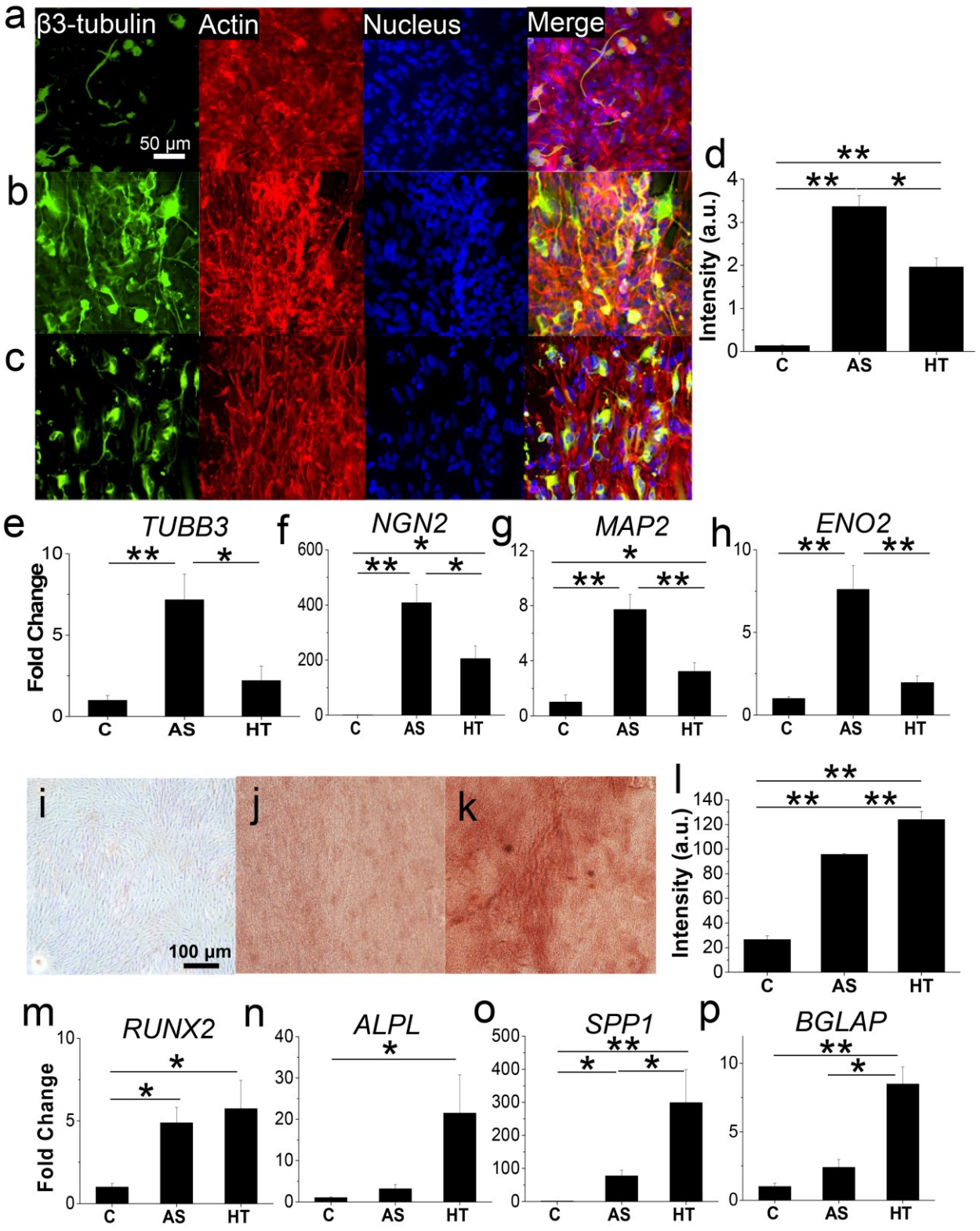


**Figure 8. Piezoelectric orientation-dependent stem cell behaviors.** (a-c) Immunofluorescence images of human neural stem cells (NSCs) cultured on (a) tissue culture plate, (b) as-spun, or (c) 65 °C heat-treated PLLA nanofibers for 1 week. TUJ. 1 (β3-tubulin, green) was used to detect cells differentiated to neurons. Cells were also counterstained with phalloidin and DAPI for the

visualization of actin and nucleus, respectively. (d) Fluorescent intensity quantification of Tuj.1 (n=5). C denotes the control group where cells were cultured on a tissue culture plate. AS and HT denote as-spun and 65 °C heat-treated PLLA nanofibers, respectively. All cells were cultured in neural stem cell growth media. (e-h) Gene expression of neuronal differentiation markers, (e) *TUBB3*, (f) *NGN2*, (g) *MAP2*, and (h) *ENO2* in hNSCs cultured on either as-spun or 65 °C heat-treated PLLA nanofibers for 1 week as compared to those cultured on a tissue culture plate. (n = 6, * and ** denote statistical significance of $p < 0.05$ and $p < 0.01$, respectively). (i-k) Histological images of human mesenchymal stem cells (hMSCs) cultured on (i) tissue culture plate, (j) as-spun, or (k) 65 °C heat-treated PLLA nanofibers for 2 weeks. Alizarin red was used to detect calcium deposits. (l) Quantification of alizarin red staining (n=5). All cells were cultured in osteogenic differentiation media. (m-p) Gene expression of osteogenic markers, (m) *RUNX2*, (n) *ALPL*, (o) *SPP1*, and (p) *BGLAP* in hMSCs cultured on either as-spun or 65 °C heat-treated PLLA nanofibers for 1 week as compared to those cultured on a tissue culture plate.

## 4. Conclusion

In summary, a DOE was used to precisely optimize the electrospinning conditions for the synthesis of uniform PLLA nanofibers having an average fiber diameter from 30 nm to 500 nm. The transverse and longitudinal piezoelectric voltage outputs of these electrospun PLLA nanofibers significantly depended on fiber diameter and heat treatment temperature. Specifically, an increase of the heat treatment temperature above the glass transition point of PLLA nanofibers greatly reduced the transverse voltage output while increasing the longitudinal voltage output. The phase content change modulated by dimensional control and heat treatment was shown to be responsible for the orientation-specific piezoelectric performance. Such modulation of piezoelectric properties in PLLA nanofibers significantly affected the differentiation behaviors of stem cells in a cell type-specific manner, where neurogenesis and osteogenesis were enhanced by orthogonal and shear piezoelectricity, respectively. Overall, our study demonstrates that the electrospun PLLA nanofibers, with precisely controlled piezoelectric properties through a systematic approach, have the potential for self-powered stem cell engineering platforms specific to target tissues.

## Conflicts of interest

There are no conflicts to declare.

**Acknowledgements**

This work was supported by the Creative Materials Discovery Program through the National Research Foundation of Korea funded by the Ministry of Science and ICT (2018M3D1A1057844) and the National Science Foundation (CBET-1805975).

**References**


[1] J. Sirohi, I. Chopra, Fundamental understanding of piezoelectric strain sensors, J Intel Mat Syst Str 11(4) (2000) 246-257

[2] C. Dagdeviren, P. Joe, O.L. Tuzman, K.I. Park, K.J. Lee, Y. Shi, Y.G. Huang, J.A. Rogers, Recent progress in flexible and stretchable piezoelectric devices for mechanical energy harvesting, sensing and actuation, Extreme Mech Lett 9 (2016) 269-281

[3] G. Ico, A. Showalter, W. Bosze, S.C. Gott, B.S. Kim, M.P. Rao, N.V. Myung, J. Nam, Size-dependent piezoelectric and mechanical properties of electrospun P(VDF-TrFE) nanofibers for enhanced energy harvesting, J Mater Chem A 4(6) (2016) 2293-2304

[4] M. Lee, C.Y. Chen, S. Wang, S.N. Cha, Y.J. Park, J.M. Kim, L.J. Chou, Z.L. Wang, A Hybrid Piezoelectric Structure for Wearable Nanogenerators, Adv Mater 24(13) (2012) 1759-1764

[5] T. Jariwala, G. Ico, Y. Tai, H. Park, N.V. Myung, J. Nam, Mechano-Responsive Piezoelectric Nanofiber as an On-Demand Drug Delivery Vehicle, ACS Applied Bio Materials 4(4) (2021) 3706-3715

[6] M.T. Chorsi, E.J. Curry, H.T. Chorsi, R. Das, J. Baroody, P.K. Purohit, H. Ilies, T.D. Nguyen, Piezoelectric Biomaterials for Sensors and Actuators, Adv Mater 31(1) (2019)

[7] X.Z. Chen, M. Hoop, N. Shamsudhin, T.Y. Huang, B. Ozkale, Q. Li, E. Siringil, F. Mushtaq, L. Di Tizio, B.J. Nelson, S. Pane, Hybrid Magnetoelectric Nanowires for Nanorobotic Applications: Fabrication, Magnetoelectric Coupling, and Magnetically Assisted In Vitro Targeted Drug Delivery, Adv Mater 29(8) (2017)

[8] S.B. Lang, Pyroelectric Effect in Bone and Tendon, Nature 212(5063) (1966) 705-&

[9] H. Athenstaedt, H. Claussen, D. Schaper, Epidermis of Human-Skin - Pyroelectric and Piezoelectric Sensor Layer, Science 216(4549) (1982) 1018-1020

[10] Z. Yin, X. Chen, J.L. Chen, W.L. Shen, T.M.H. Nguyen, L. Gao, H.W. Ouyang, The regulation of tendon stem cell differentiation by the alignment of nanofibers, Biomaterials 31(8) (2010) 2163-2175

[11] N.H. Zhang, Inverse Piezoelectricity of Single-Stranded DNA Film on Microcantilever, Ieee T Dielect El In 22(3) (2015) 1376-1380

[12] S.H. Bhang, W.S. Jang, J. Han, J.K. Yoon, W.G. La, E. Lee, Y.S. Kim, J.Y. Shin, T.J. Lee, H.K. Baik, B.S. Kim, Zinc Oxide Nanorod-Based Piezoelectric Dermal Patch for Wound Healing, Adv Funct Mater 27(1) (2017)

[13] J. Jacob, N. More, K. Kalia, G. Kapusetti, Piezoelectric smart biomaterials for bone and cartilage tissue engineering, Inflamm Regen 38 (2018)

[14] T. Karaki, K. Yan, T. Miyamoto, M. Adachi, Lead-free piezoelectric ceramics with large dielectric and piezoelectric constants manufactured from BaTiO3 nano-powder, Jpn J Appl Phys 2 46(4-7) (2007) L97-L98

[15] C.N. Xu, M. Akiyama, K. Nonaka, T. Watanabe, Electrical power generation characteristics of PZT piezoelectric ceramics, Ieee T Ultrason Ferr 45(4) (1998) 1065-1070

[16] M. Akiyama, T. Kamohara, K. Kano, A. Teshigahara, Y. Takeuchi, N. Kawahara, Enhancement of Piezoelectric Response in Scandium Aluminum Nitride Alloy Thin Films Prepared by Dual Reactive Cosputtering, Adv Mater 21(5) (2009) 593-+

[17] G. Ico, A. Myung, B.S. Kim, N.V. Myung, J. Nam, Transformative piezoelectric enhancement of P(VDF-TrFE) synergistically driven by nanoscale dimensional reduction and thermal treatment, Nanoscale 10(6) (2018) 2894-2901

[18] L.J. Lu, B. Yang, Y.Q. Zhai, J.Q. Liu, Electrospinning core-sheath piezoelectric microfibers for self-powered stitchable sensor, Nano Energy 76 (2020)
[19] L.J. Lu, W.Q. Ding, J.Q. Liu, B. Yang, Flexible PVDF based piezoelectric nanogenerators, Nano Energy 78 (2020)
[20] Y. Tai, G. Ico, K. Low, J. Liu, T. Jariwala, D. Garcia-Viramontes, K.H. Lee, N.V. Myung, B.H. Park, J. Nam, Formation of 3D Self-Organized Neuron-Glial Interface Derived from Neural Stem Cells via Mechano-Electrical Stimulation, Adv Healthc Mater (2021)
[21] S. Sasaki, T. Asakura, Helix distortion and crystal structure of the alpha-form of poly(L-lactide), Macromolecules 36(22) (2003) 8385-8390
[22] H. Wang, J.M. Zhang, K. Tashiro, Phase Transition Mechanism of Poly(L-lactic acid) among the alpha, delta, and beta Forms on the Basis of the Reinvestigated Crystal Structure of the beta Form, Macromolecules 50(8) (2017) 3285-3300
[23] M. Minary-Jolandan, M.F. Yu, Shear piezoelectricity in bone at the nanoscale, Appl Phys Lett 97(15) (2010)
[24] Y. Ikarashi, T. Tsuchiya, A. Nakamura, Effect of heat treatment of poly(L-lactide) on the response of osteoblast-like MC3T3-E1 cells, Biomaterials 21(12) (2000) 1259-1267
[25] A. Sultana, S.K. Ghosh, V. Sencadas, T. Zheng, M.J. Higgins, T.R. Middya, D. Mandal, Human skin interactive self-powered wearable piezoelectric bio-e-skin by electrospun poly-L-lactic acid nanofibers for non-invasive physiological signal monitoring, J Mater Chem B 5(35) (2017) 7352-7359
[26] G.R. Zhao, B.S. Huang, J.X. Zhang, A.C. Wang, K.L. Ren, Z.L. Wang, Electrospun Poly(l-Lactic Acid) Nanofibers for Nanogenerator and Diagnostic Sensor Applications, Macromol Mater Eng 302(5) (2017)
[27] D. Arbeiter, K. Schümann, O. Sahmel, T. Eickner, K.-P. Schmitz, N. Grabow, The effect of thermal treatment on the mechanical properties of PLLA tubular specimens, Current Directions in Biomedical Engineering 2(1) (2016) 27-29
[28] N. Bassiri-Gharb, I. Fujii, E. Hong, S. Trolier-McKinstry, D.V. Taylor, D. Damjanovic, Domain wall contributions to the properties of piezoelectric thin films, J Electroceram 19(1) (2007) 49-65
[29] L. Fambri, A. Pegoretti, R. Fenner, S.D. Incardona, C. Migliaresi, Biodegradable fibres of poly(L-lactic acid) produced by melt spinning, Polymer 38(1) (1997) 79-85
[30] K. Mezghani, J.E. Spruiell, High speed melt spinning of poly(L-lactic acid) filaments, J Polym Sci Pol Phys 36(6) (1998) 1005-1012
[31] B. Wunderlich, Teaching thermal analysis of polymeric materials, J Therm Anal Calorim 59(1-2) (2000) 7-19
[32] F.H. Sanchez, J.M. Mateo, F.J.R. Colomer, M.S. Sanchez, J.L.G. Ribelles, J.F. Mano, Influence of low-temperature nucleation on the crystallization process of poly(L-lactide), Biomacromolecules 6(6) (2005) 3283-3290
[33] S. Xie, A. Gannepalli, Q.N. Chen, Y. Liu, Y. Zhou, R. Proksch, J. Li, High resolution quantitative piezoresponse force microscopy of BiFeO 3 nanofibers with dramatically enhanced sensitivity, Nanoscale 4(2) (2012) 408-413
[34] M. Maldonado, L.Y. Wong, C. Echeverria, G. Ico, K. Low, T. Fujimoto, J.K. Johnson, J. Nam, The effects of electrospun substrate-mediated cell colony morphology on the self-renewal of human induced pluripotent stem cells, Biomaterials 50 (2015) 10-19
[35] M. Maldonado, L.Y. Wong, C. Echeverria, G. Ico, K. Low, T. Fujimoto, J.K. Johnson, J. Nam, The effects of electrospun substrate-mediated cell colony morphology on the self-renewal of

human induced pluripotent stem cells, Biomaterials 50 (2015) 10-9.10.1016/j.biomaterials.2015.01.037
[36] P. Martin-Maestro, A. Sproul, H. Martinez, D. Paquet, M. Gerges, S. Noggle, A.A. Starkov, Autophagy Induction by Bexarotene Promotes Mitophagy in Presenilin 1 Familial Alzheimer's Disease iPSC-Derived Neural Stem Cells, Mol Neurobiol 56(12) (2019) 8220-8236.10.1007/s12035-019-01665-y
[37] T. Fu, X.B. Tang, Z.K. Cai, Y. Zuo, Y.M. Tang, X.H. Zhao, Correlation research of phase angle variation and coating performance by means of Pearson's correlation coefficient, Prog Org Coat 139 (2020)
[38] P. Shirazi, G. Ico, C.S. Anderson, M.C. Ma, B.S. Kim, J. Nam, N.V. Myung, Size-Dependent Piezoelectric Properties of Electrospun BaTiO3 for Enhanced Energy Harvesting, Adv Sustain Syst 1(11) (2017)
[39] R. Inai, M. Kotaki, S. Ramakrishna, Structure and properties of electrospun PLLA single nanofibres, Nanotechnology 16(2) (2005) 208-213
[40] X.H. Zong, K. Kim, D.F. Fang, S.F. Ran, B.S. Hsiao, B. Chu, Structure and process relationship of electrospun bioabsorbable nanofiber membranes, Polymer 43(16) (2002) 4403-4412
[41] C. Ribeiro, V. Sencadas, C.M. Costa, J.L.G. Ribelles, S. Lanceros-Mendez, Tailoring the morphology and crystallinity of poly(L-lactide acid) electrospun membranes, Sci Technol Adv Mat 12(1) (2011)
[42] M.V. Kakade, S. Givens, K. Gardner, K.H. Lee, D.B. Chase, J.F. Rabolt, Electric field induced orientation of polymer chains in macroscopically aligned electrospun polymer nanofibers, J Am Chem Soc 129(10) (2007) 2777-2782
[43] J. Ma, Q. Zhang, A. Mayo, Z.H. Ni, H. Yi, Y.F. Chen, R. Mu, L.M. Bellan, D.Y. Li, Thermal conductivity of electrospun polyethylene nanofibers, Nanoscale 7(40) (2015) 16899-16908
[44] O. Ero-Phillips, M. Jenkins, A. Stamboulis, Tailoring Crystallinity of Electrospun Plla Fibres by Control of Electrospinning Parameters, Polymers-Basel 4(3) (2012) 1331-1348
[45] E.J. Curry, T.T. Le, R. Das, K. Ke, E.M. Santorella, D. Paul, M.T. Chorsi, K.T.M. Tran, J. Baroody, E.R. Borges, B. Ko, A. Golabchi, X.N. Xin, D. Rowe, L.X. Yue, J.L. Feng, M.D. Morales-Acosta, Q. Wu, I.P. Chen, X.T. Cui, J. Pachter, T.D. Nguyen, Biodegradable nanofiber-based piezoelectric transducer, P Natl Acad Sci USA 117(1) (2020) 214-220
[46] A.H. Rajabi, M. Jaffe, T.L. Arinzeh, Piezoelectric materials for tissue regeneration: A review, Acta Biomater 24 (2015) 12-23
[47] H. Yuan, T.M. Lei, Y. Qin, J.H. He, R.S. Yang, Design and application of piezoelectric biomaterials, J Phys D Appl Phys 52(19) (2019)
[48] Y.S. Lee, T.L. Arinzeh, The Influence of Piezoelectric Scaffolds on Neural Differentiation of Human Neural Stem/Progenitor Cells, Tissue Eng Pt A 18(19-20) (2012) 2063-2072
[49] B. Tandon, J.J. Blaker, S.H. Cartmell, Piezoelectric materials as stimulatory biomedical materials and scaffolds for bone repair, Acta Biomater 73 (2018) 1-20
[50] C.J. Wilson, Y. Kawaguchi, The origins of two-state spontaneous membrane potential fluctuations of neostriatal spiny neurons, J Neurosci 16(7) (1996) 2397-2410
[51] Y. Cheng, Y. Xu, Y. Qian, X. Chen, Y.M. Ouyang, W.E. Yuan, 3D structured self-powered PVDF/PCL scaffolds for peripheral nerve regeneration, Nano Energy 69 (2020)
[52] G. Murillo, A. Blanquer, C. Vargas-Estevez, L. Barrios, E. Ibanez, C. Nogues, J. Esteve, Electromechanical Nanogenerator-Cell Interaction Modulates Cell Activity, Adv Mater 29(24) (2017)

[53] X.D. Zhang, X. Cui, D.C. Wang, S. Wang, Z.R. Liu, G.R. Zhao, Y. Zhang, Z. Li, Z.L. Wang, L.L. Li, Piezoelectric Nanotopography Induced Neuron-Like Differentiation of Stem Cells, Adv Funct Mater 29(22) (2019)
[54] C.A. Lemmon, N.J. Sniadecki, S.A. Ruiz, J.L. Tan, L.H. Romer, C.S. Chen, Shear force at the cell-matrix interface: enhanced analysis for microfabricated post array detectors, Mechanics & chemistry of biosystems: MCB 2(1) (2005) 1

Vitae

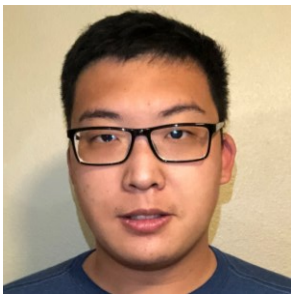

Youyi Tai is a Ph.D. student in the Department of Bioengineering at University of California, Riverside.

Steve Yang is a Ph.D. student in the Department of Materials Science and Engineering at University of California, Riverside.

Dr. Sooyoun Yu is a postdoctoral researcher in the Department of Chemical and Biomolecular Engineering at University of Notre Dame. She received her Ph.D. in Chemical and Environmental Engineering at University of California, Riverside in 2020. Her research interests are in electrospun nanofibers for applications in energy and environment.

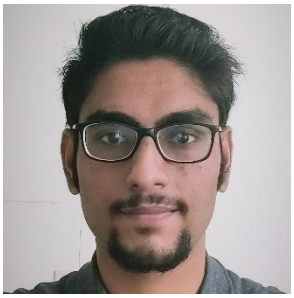

Aihik Banerjee is a Ph.D. student in the Department of Bioengineering at University of California, Riverside.

Prof. Nosang Vincent Myung is Bernard Keating Crawford Endowed Professor in Chemical and Biomolecular Engineering at University of Notre Dame. He received his Ph.D. in Chemical Engineering at University of California, Los Angeles in 1998. His lab is based on nano-enabled materials for applications in energy and environment.

Prof. Jin Nam is an Associate Professor in the Department of Bioengineering at University of California, Riverside. He received his Ph.D. in Materials Science and Engineering at the Ohio State University in 2006. His lab focuses on developing enabling technologies to repair damaged tissues via stem cell/tissue engineering approaches.